Petroleum Science 23 (2026) 2902–2915

Contents lists available at ScienceDirect

Petroleum Science

journal homepage: www.keaipublishing.com/en/journals/petroleum-science

Original Paper

Effect of cashew nutshell liquid-modified EVAL on flow behavior and crystallization of waxy systems

Zheng-Nan Sun [a,*], Pei-Song Shi [a], Yi-Hai Yang [a], Ming-Xing Bai [b], Guo-Lin Jing [a,**], Cai-Yu Guan [a]

[a] Provincial Key Laboratory of Oil & Gas Chemical Technology, College of Chemistry & Chemical Engineering, Northeast Petroleum University, Daqing, 163318, Heilongjiang, China
[b] School of Petroleum Engineering, Northeast Petroleum University, Daqing, 163318, Heilongjiang, China

ARTICLE INFO

Article history:
Received 8 June 2025
Received in revised form
15 October 2025
Accepted 13 January 2026
Available online 17 January 2026

Edited by Teng Zhu and Meng-Jiao Zhou

Keywords:
Pour point depressants
EVAL
Anacardic acid
Chemical grafting
Cold-flow properties
Crystallization behavior

ABSTRACT

Light crude oils are being progressively depleted as the dominant primary energy source, leading to increased attention on the extraction and utilization of highly waxy crude oils. To address the poor low-temperature fluidity of waxy crude oil, cashew nut shell liquid (CNSL), which is rich in anacardic acid, was extracted from low-cost and renewable cashew nut shells and subsequently modified with EVAL through esterification at different mass ratios (mEVAL:mCNSL = 1:1, 1:2, 1:3) to synthesize the EVAL-g-AAC pour point depressant. Chemical structure characterization confirmed the successful grafting of EVAL with anacardic acid. The experimental results demonstrated that EVAL-g-AAC 2 (mEVAL:mCNSL = 1:2) exhibited the best pour point-reducing performance at a dosage of 400 ppm, lowering the pour point of waxy model oils by 24 °C. This reduction was 8 °C and 5 °C greater than that achieved by EVA and EVAL, respectively. In addition, its viscosity reduction rate increased by 28.5% relative to EVAL, while simultaneously decreasing the gelation temperature and viscoelastic properties of the model oils. Additionally, the low-temperature crystallization behavior of wax crystals was investigated using polarized optical microscopy (POM), differential scanning calorimetry (DSC), and X-ray diffraction (XRD). It proposed a possible mechanism of action for the new pour point depressant through the "alkyl long-chain promotes co-crystallization formation, polar groups promote dispersion, and rigid structure promotes nucleation" triple synergy to improve the crystallization behavior of wax molecules.

1. Introduction

Petroleum remains the world's largest primary energy source. With advances in the petrochemical industry and modern technology, light crude oil resources are being progressively depleted, while the demand for fossil energy continues to be indispensable for industrial production, transportation, and residential electricity supply (Anghelache et al., 2023; Khatri et al., 2022). Heavy oil reservoirs are widely distributed worldwide (Zhang et al., 2024). In China, crude oil production is dominated by waxy crude oils, which are characterized by high wax content, elevated pour points, and high viscosity (Yin et al., 2024). As the world's largest importer of crude oil, China relies heavily on pipeline transportation. However, during pipeline transport of waxy crude oil, temperature differences between the interior and exterior of the pipeline cause paraffin molecules to crystallize as the oil cools. Due to the temperature gradient, wax crystals precipitate from crude oil near the pipeline wall. The three-dimensional network structure formed during wax crystal precipitation promotes cross-linking among wax molecules, which significantly reduces the fluidity of the crude oil. This not only increases the difficulty of crude oil storage and transportation but also elevates operational risks as wax deposition accumulates on the inner wall of the pipeline (Li et al., 2024b; Liu et al., 2025). This not only increases crude oil transportation costs but also introduces safety risks. To

* Corresponding author.
** Corresponding author.
E-mail addresses: sunzhengnan@nepu.edu.cn (Z.-N. Sun), jglxueshu@yeah.net (G.-L. Jing).

Peer review under the responsibility of China University of Petroleum (Beijing).

https://doi.org/10.1016/j.petsci.2026.01.017

address these issues, physical or chemical methods can be employed. Physical approaches aim to enhance the fluidity of crude oil within pipelines by preheating the pipeline, improving thermal insulation performance, applying electromagnetic treatments, or diluting the waxy crude oil (Muñoz and Ancheyta, 2024; Sun et al., 2024a; Xie et al., 2025). The preheating of oil pipelines offers several advantages, including technical maturity, strong adaptability, and independence from crude oil composition, while also preserving the chemical composition of the crude oil. However, this method suffers from high energy consumption, significant heat loss, substantial capital investment, safety concerns, and elevated carbon emissions. Consequently, it is mainly applicable to short-distance transportation systems, such as oilfield gathering and transfer operations, or to heavy crude oils. In addition, ultrasonic treatment for viscosity reduction provides the benefits of rapid effectiveness and a purely physical process that requires no chemical additives. However, this technique has several limitations, including a narrow scope of application, poor persistence of its effects, high equipment costs, and difficulties associated with large-scale implementation. Therefore, it is most suitable for removing blockages near oil wells, for use in short-distance and small-diameter gathering pipelines, or as a pre-treatment method in combination with other approaches (such as chemical additives) (Dengaev et al., 2023; Yang et al., 2025a). For chemical methods, the low-temperature fluidity of waxy crude oil can be enhanced by adding PPDs, polymer drag-reducing agents, or by employing microbial anti-waxing techniques (Du et al., 2024; Yang et al., 2025b; Yao et al., 2022). The use of PPDs offers several advantages, including energy conservation, reduced emissions, low dosage requirements, cost-effectiveness, operational simplicity, and automation, as well as effective enhancement of the low-temperature flow properties of waxy crude oil. However, variations in the content of asphaltenes and wax in crude oil can limit the efficacy of PPDs, and their performance may decline over time. Consequently, PPDs are particularly suitable for the stable transportation of heavy crude oils. PPDs can also serve as an auxiliary measure for heated transportation by reducing operating temperatures and improving the pipeline's ability to restart after shutdown. Among the various solutions, the addition of PPDs to waxy crude oil offers advantages such as simplicity, high efficiency, broad applicability, and low cost, making it the primary method for enhancing the low-temperature fluidity of waxy crude oil in pipelines (Li et al., 2024a; Zhu et al., 2025).

The primary PPDs currently used in waxy crude oils are EVA copolymers. EVA is among the most widely used PPDs in commercial applications; however, its effectiveness in reducing the pour point of crude oils with high wax and asphaltene contents remains limited. Consequently, modifying existing PPDs to meet practical production requirements has become a central focus of research (Kuzmin et al., 2024; Ragab et al., 2025; Sun et al., 2023). Some researchers have employed alcoholysis modification of EVA or grafting with maleic anhydride to increase the polarity of EVA, thereby enhancing its dispersibility on wax crystals (Liu et al., 2021; Zhang et al., 2023). Others have explored nano-hybrid modification of EVA to promote heterogeneous nucleation on wax crystals (Liu et al., 2023; Xia et al., 2022b; Yan et al., 2024; Yang et al., 2025c; Yao et al., 2018), further improving the low-temperature fluidity of crude oil. However, the increased polarity of alcoholysis-modified EVA reduces its solubility in crude oil and weakens its co-crystallization with wax crystals. Meanwhile, EVA modified via nanohybridization can hinder subsequent crude oil processing due to high levels of nanoparticle incorporation. Therefore, enhancing EVA''s polarity while simultaneously strengthening its co-crystallization and nucleation interactions with wax crystals is crucial for improving the applicability of EVA-based PPDs in crude oil.

Biomass-based materials, as environmentally friendly and renewable resources, provide novel opportunities for designing flow modifiers for petroleum products due to their unique chemical compositions. Some studies have shown that fatty acid alkyl chains extracted from plants and animals can modify the morphology of wax crystals through co-crystallization with wax molecules, thereby improving the low-temperature flow properties of oils (Shittu and Achugasim, 2023; Xue et al., 2016). Additionally, research by Kuzmin et al. (Kuzmin et al., 2025; Sultanbekov and Schipachev, 2022) demonstrates that incorporating waste cooking oil into fuels allows the fatty acid esters it contains to adsorb onto the surfaces of asphaltene aggregates within the fuel medium. This process forms stable micelles, preventing the formation of large aggregates and their subsequent congealment and precipitation, which can negatively impact fuel fluidity. Xu et al. (2023) extracted trans-anethole containing carboxyl groups from natural *Illicium verum* and copolymerized it with methacrylate. The nonpolar groups of the resulting copolymer facilitate co-crystallization with wax crystals, while the polar groups disperse the wax crystals and alter their growth direction, enabling its use as a pour point depressant (Modi and Nagar, 2024; Uzoh et al., 2025). However, an additive dosage of 2000 mg/kg is required to achieve the most effective improvement in the low-temperature flow properties of diesel fuel. In recent years, Marenov et al. (2020) isolated crude gossypol (CG) from refined cottonseed oil soapstock and blended it with EVA to produce a composite pour point depressant for crude oil. This formulation inhibits wax crystal growth, achieving a maximum pour point reduction of 12 °C. Additionally, extracting active components from agricultural byproducts, such as cashew nut shells, offers a cost-effective and renewable approach. Cashew nut shells are inexpensive, readily available, and ecologically sustainable, demonstrating significant potential as biological raw materials for the large-scale preparation of PPDs. CNSL extracted from cashew nut shells contains anacardic acid, cardanol, cardol, and 2-methyl cardol, with the chemical structures of each component shown in Fig. 1. CNSL obtained using a low-boiling solvent is particularly rich in anacardic acid (Eke et al., 2021), which possesses polar groups such as hydroxyl and carboxyl, as well as a distinctive molecular structure featuring a benzene ring and a long alkyl chain. Some studies have reported that directly doping CNSL into crude oil as a pour point depressant requires a high dosage to achieve effective improvement of the low-temperature fluidity of the oil (Eke et al., 2021; Pandian et al., 2021). The hydroxyl and carboxyl groups of anacardic acid molecules in cashew nut-shell liquid provide a basis for developing novel PPDs.

In this study, CNSL was extracted from discarded cashew nut shells using a low-boiling-point polar solvent, yielding a material rich in anacardic acid. The benzene ring of anacardic acid provides a rigid structure that can act as a nucleating agent for wax crystals (Lin et al., 2020; Yin et al., 2020), while its long alkyl chains can co-crystallize with wax crystals in model oil (Wang et al., 2024). Additionally, the polar groups of anacardic acid can disperse wax crystals (Cui et al., 2024). Therefore, CNSL rich in anacardic acid was chosen for modification and grafting onto EVA (i.e., EVAL) following alcoholic hydrolysis. In this study, AAC-modified grafted EVAL (EVAL-g-AAC) was synthesized for the first time, and its potential as a coagulant reducer with industrial application prospects was evaluated. EVA, EVAL, and EVAL-g-AAC were characterized using Fourier-transform infrared spectroscopy (FTIR) and ^{1}H NMR. Their

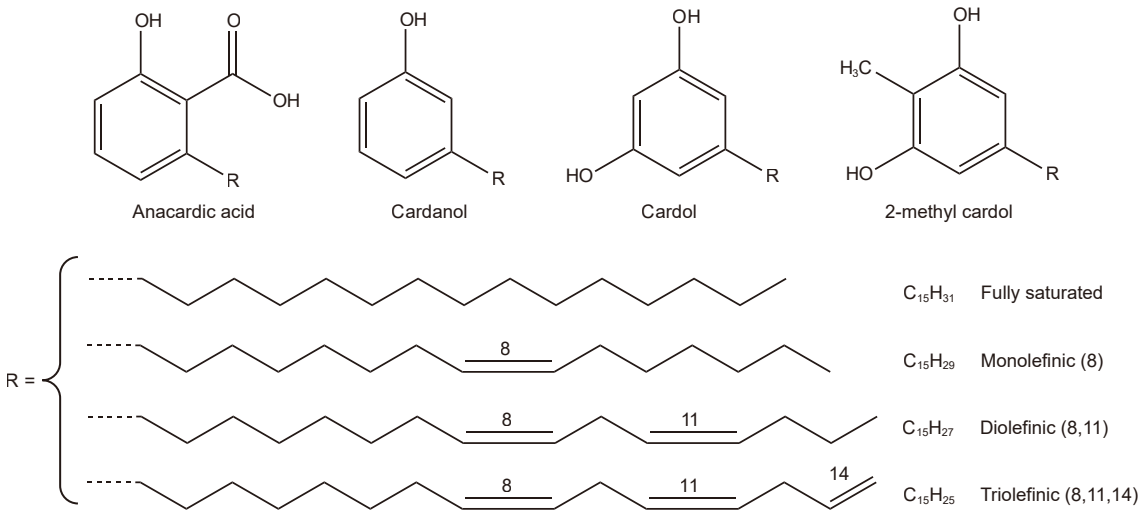

Fig. 1. Chemical structure of components in CNSL.

effects on the rheological behavior of waxy model oil were subsequently investigated. Additionally, X-ray diffraction (XRD), thermal analysis, and microstructural observations of wax crystals in the model oil, before and after doping with the pour point depressant, were combined to elucidate the mechanism of EVAL-g-AAC on the low-temperature flow behavior of waxy model oil.

2. Experiment

2.1. Materials

The materials used in this study included light crude oil and 58# paraffin (provided by Daqing Petrochemical Company No. 137, with a melting point of 58 °C), cashew nut shells from Cambodia, acetone, EVA (vinyl acetate 32 wt%, melting index 43 g/10 min), methanol, toluene, and sodium hydroxide. All reagents and chemicals employed in the experiments were of analytical grade.

2.2. Sample preparation

2.2.1. Preparation for waxy model oil

The light crude oil was mixed with paraffin wax supplied by Daqing Petrochemical Company and continuously stirred and dissolved at 60 °C for 2 h, resulting in a model oil system with a high wax content of 17.16 wt%. The physical properties of the model oil are summarized in Table 1. The carbon number distribution of the model oil was determined using gas chromatography (GC), and the results are presented in Fig. 2. As shown in Fig. 2(a), the light oil is concentrated in the low carbon number range (C6–C10), which is consistent with the main components of light crude oils, primarily complex alkanes with carbon numbers between C6 and C15. As shown in Fig. 2(b) and (c), after paraffin was added and dissolved in light crude oil, the concentrated carbon number distribution in the C25–C40 range corresponds to the added paraffin. In crude oil, wax refers to a hydrocarbon mixture containing more than 16 carbon atoms, with C16–C36 generally classified as paraffin. This fraction is primarily composed of n-alkanes, with smaller amounts of isoparaffins and aromatic hydrocarbons.

2.2.2. Extraction of CNSL

When CNSL is extracted using a Soxhlet extractor with a low-boiling-point solvent, the anacardic acid content in the resulting CNSL is approximately 80% (Eke et al., 2021, 2024; Koteich Khatib et al., 2020). In this study, acetone, a low-boiling-point and highly polar solvent, was selected as the extractant for Soxhlet extraction. Compared with other methods, this approach yields CNSL with a higher anacardic acid content, lower cost, and a simpler operational procedure, as illustrated in Fig. 3. Following the procedures reported in the literature (Eke et al., 2024; Gandhi et al., 2013), the cashew nutshells were first washed to remove mechanical impurities and then air-dried at 60 °C for 3 h in a blast drying oven to obtain CNSL rich in anacardic acid. After drying, 30 g of cashew nutshells were weighed and placed in a Soxhlet extractor, followed by the addition of 200 mL of acetone. Extraction was carried out at 65 °C for 6 h using repeated cycles of solvent reflux. At the end of the extraction, the remaining solvent in the extractor was returned to the round-bottom flask, and the extracted cashew shells were replaced with 30 g of fresh, unextracted shells. This extraction process was repeated until the low-boiling-point solvent was nearly saturated with CNSL. After extraction, the solution was collected and filtered through a rapid quantitative filter paper to remove residual mechanical impurities, such as cashew nutshell flocs. The acetone solvent was then separated and recovered using a vacuum rotary evaporator at 50 °C based on its relative volatility, allowing the solvent to be recycled. Finally, the concentrated extract remaining in the rotary flask was collected to obtain cashew nut-shell liquid (CNSL) enriched with anacardic acid.

2.2.3. Alcoholysis of EVA

Two grams of EVA were weighed into a three-necked flask, and 25 mL of toluene was added as the solvent. After EVA was

Table 1
Physical characteristics of waxy model oil.

Total paraffin content, wt%	Asphaltene, wt%	Resin, wt%	Pour point, °C	ρ_4^{20}, g/cm^3	Sulfur content, wt%	Flash point, °C
17.16	1.38	10.34	35	0.829	0.58	52

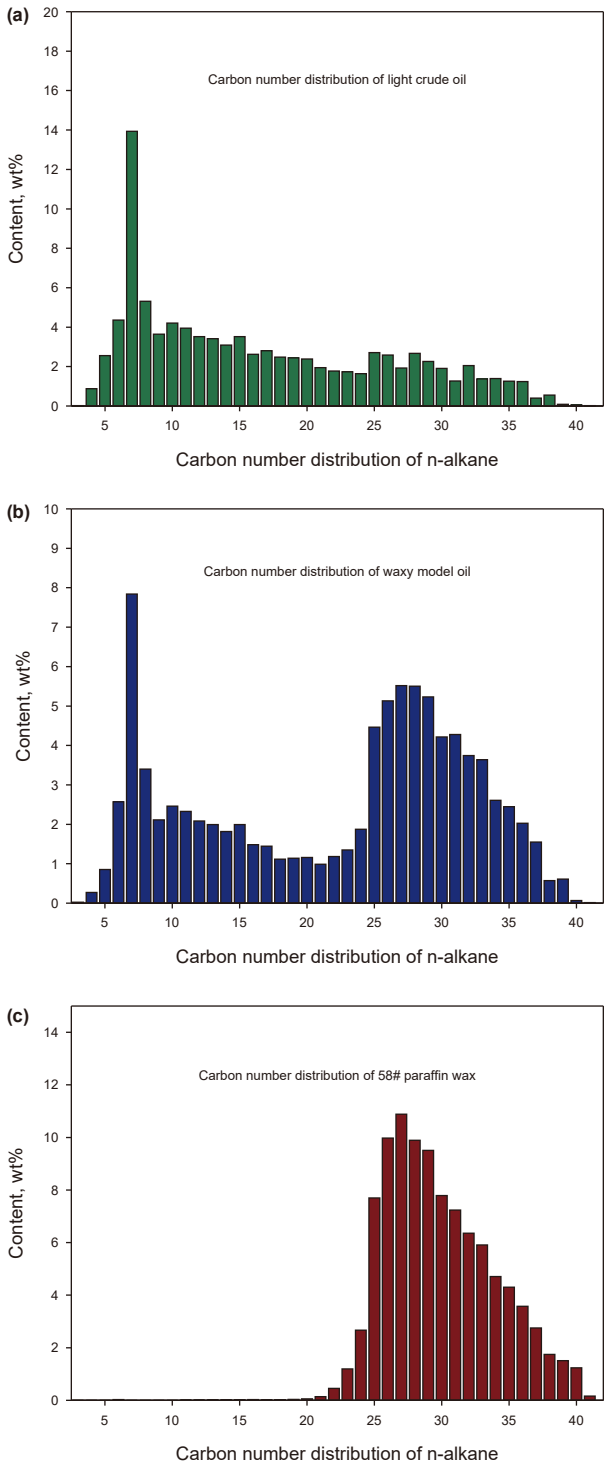

Fig. 2. Carbon number distribution of **(a)** light crude oil, **(b)** waxy model oil, and **(c)** 58# paraffin wax.

completely dissolved, 20 mL of methanol was added, and the mixture was magnetically stirred at 60 °C for 30 min. A 5 g/L sodium hydroxide solution was then added dropwise as a catalyst at a rate of 1–2 drops per second, and the reaction was carried out at 45 °C for 3 h. After completion, the product was filtered and washed three times with methanol to remove CH_3COOCH_3, followed by drying in a vacuum oven at 60 °C for 24 h to remove any residual solvent. The resulting product was alcoholized EVA (EVAL), and the reaction mechanism is illustrated in Fig. 4 (Liu et al., 2021).

2.2.4. Preparation of EVAL-g-AAC pour point depressant

EVAL and CNSL were dissolved in toluene at mass ratios of mEVAL:mCNSL = 1:1, 1:2, and 1:3, and the mixtures were continuously stirred at 90 °C for 6 h. After the reaction, the products were washed three times with ice-cold methanol to remove other impurities from CNSL, then filtered and collected. The collected products were dried in a vacuum oven at 80 °C for 24 h to remove residual solvent, yielding the EVAL-g-AAC PPDs. The products synthesized at different mass ratios (mEVAL:mCNSL = 1:1, 1:2, 1:3) were designated as EVAL-g-AAC 1, EVAL-g-AAC 2, and EVAL-g-AAC 3, respectively. The reaction mechanism is illustrated in Fig. 5.

2.3. Proton nuclear magnetic resonance (^1H NMR)

The samples were dissolved in deuterated chloroform ($CDCl_3$) at a concentration of 70 mg/mL using an AVANCE III 500 nuclear magnetic resonance (NMR) spectrometer (Bruker, Germany). Tetramethylsilane (TMS) was used as the reference standard for ^1H NMR testing to analyze the chemical structures of EVA, EVAL, and EVAL-g-AAC.

2.4. Fourier transform infrared spectroscopy

A Fourier Transform Infrared Spectrometer (FTIR) model TENSOR 27 from Bruker, Germany, was used for the analysis. Prepare a thin film of the sample to be tested and cover it with a thin sheet pressed from potassium bromide (KBr) granules and powder. Conduct the test at room temperature using a wavelength range of 4000 cm^{-1} to 400 cm^{-1} to characterize the chemical functional groups of EVA, EVAL, and EVAL-g-AAC.

2.5. Deionized water contact angle measurement

A JGW-360A contact angle goniometer was used to measure the water contact angles of EVA, EVAL, and EVAL-g-AAC to evaluate and compare the polarity of these materials. The pour point depressant samples were prepared as uniform, smooth films and placed on glass slides on the sample stage. The camera of the contact angle instrument was adjusted to ensure a clear view of the sample's horizontal plane, and deionized water was delivered via a needle tube and dropped onto the sample surface to measure the water contact angles.

2.6. Pour point measurement

The pour point of the waxy model oil, both before and after the addition of the pour point depressant, was determined according to the Chinese petroleum industry standard SY/T 0541-2009. The doped and undoped model oils were preheated in a water bath at 60 °C for 20 min to ensure good fluidity. The oils were then loaded into the inner tube up to the graduated line for pour point measurement, while a thermometer was placed in the outer tube of an ice–water bath maintained at a temperature at least 8 °C below the expected pour point of the samples. The cooling rate of the oil samples was controlled at 0.5–1 °C/min, and the temperature at which the waxy model oils lost fluidity was recorded to determine the pour point of the oil samples. Each oil sample was tested three times to ensure the validity of the data from the parallel experiments, and error bars are provided in the corresponding figures.

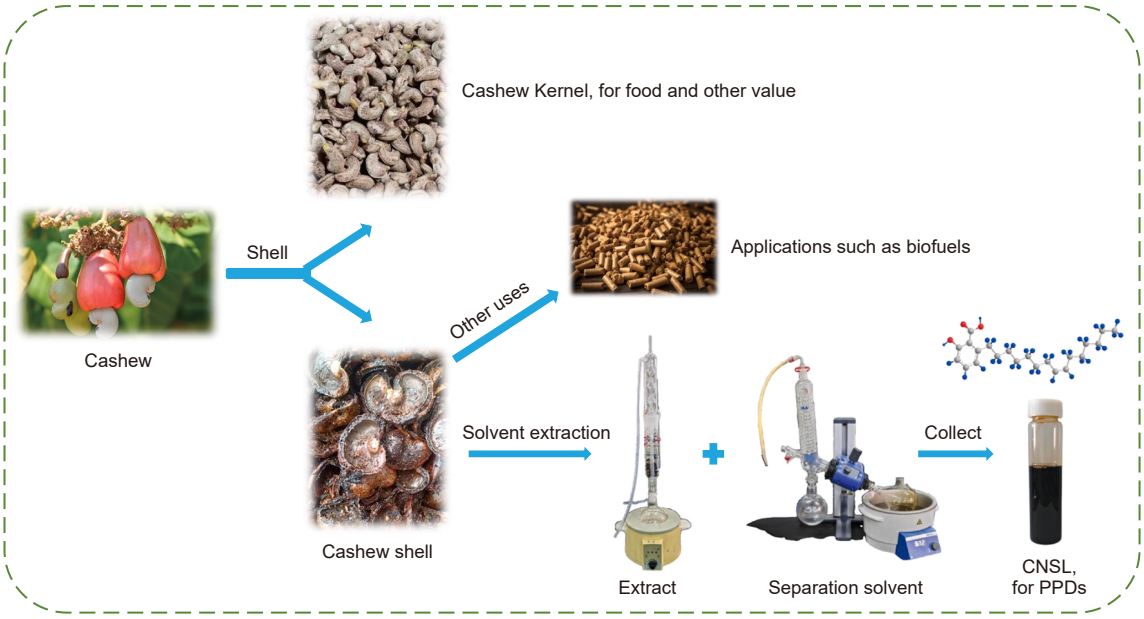

Fig. 3. CNSL extraction flow chart.

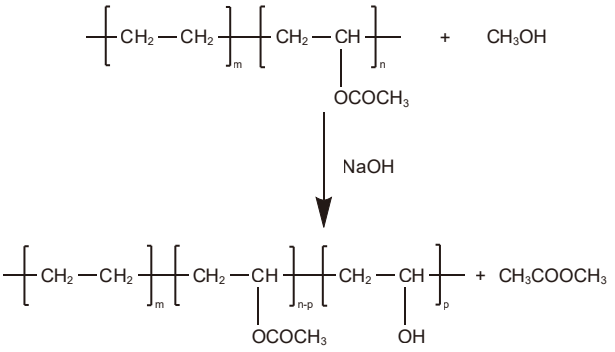

Fig. 4. Synthesis mechanism of EVAL.

2.7. The flow behavior of pure and additive model systems

The viscosity-temperature curves, variable shear viscosity curves, viscoelastic property curves, and yield stress curves of the waxy model oils, both before and after the addition of PPDs, were measured using a DISCOVERY HR-1 advanced rotational rheometer (TA Instruments, USA). The oil samples doped with different PPDs were preheated at 60 °C for 2 h to eliminate thermal history and then loaded into the rheometer for testing. Each curve represents the average of at least three highly reproducible replicate measurements.

(1) Viscosity-temperature curves: Preheat the oil sample and maintain it at a constant temperature of 60 °C for 10 min. Then, cool the sample from 60 °C to 15 °C at a rate of 1 °C/min under a constant shear rate of 50 s^{-1} to determine the apparent viscosity of the oil sample as a function of temperature.

(2) Variable shear viscosity curves: Cool the preheated oil sample at a rate of 1 °C/min from 60 °C to 15 °C, maintain the temperature at 15 °C for 10 min to form a stable gel structure, and then increase the shear rate from 20 s^{-1} to 200 s^{-1} over 10 min to determine how the viscosity of the oil sample changes with shear rate.

(3) Viscoelastic property curves: Under shear conditions of small amplitude oscillation with a control strain of 0.0005 and an oscillation frequency of 1 Hz, the preheated oil sample is cooled from 60 °C to 15 °C at a cooling rate of 1 °C/min. Based on the changes in the storage modulus and loss modulus with temperature, the temperature corresponding to $G' = G''$ is the gelation temperature of the oil sample.

(4) Yield property curves: The preheated oil sample was first maintained at a constant temperature of 60 °C for 5 min. It was then cooled from 60 °C to 15 °C at a rate of 1 °C/min and held at 15 °C for 30 min. Subsequently, over a period of 10 min, the shear rate was continuously increased from 5 s^{-1} to 200 s^{-1}, while the strain of the oil sample was recorded as a function of shear stress to obtain the stress-strain curve (Xia et al., 2022a).

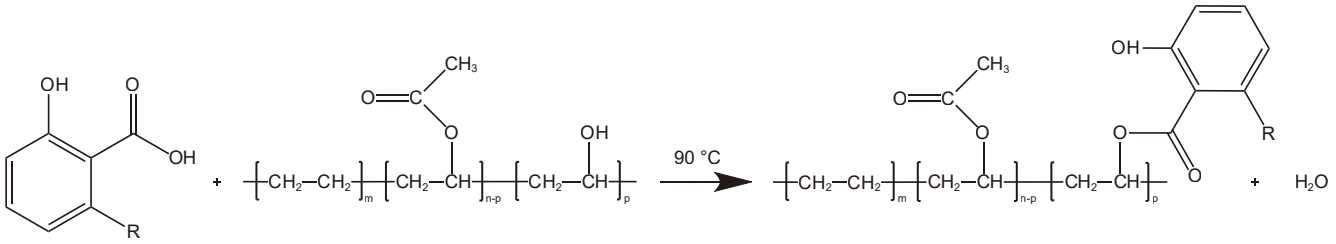

Fig. 5. Synthesis mechanism of EVAL-g-AAC.

2.8. Differential scanning calorimetry (DSC) measurement

A DSC 214 Polyma differential scanning calorimeter (NETZSCH, Germany) measures the WAT of waxy model oil before and after the addition of additives. The oil samples were heated from room temperature to 70 °C at a heating rate of 5 °C/min in an inert atmosphere and then cooled from 70 °C to −20 °C at a cooling rate of 5 °C/min. The effects of EVA, EVAL, and EVAL-g-AAC on the wax crystallization in the model oil were compared.

2.9. Microscopic observation of waxy model oil

A cross-polarized light microscope (ZEISS AXIO, Germany) equipped with an IMc 5 digital camera was used to observe the microscopic morphology of wax crystals in the initial model oil and in waxy model oils containing different PPDs. A drop of the oil sample, preheated to 60 °C, was placed on a glass slide using a hot glass rod and covered with a cover slip to ensure even distribution. The temperature was then decreased from 60 °C to 15 °C at a rate of 1 °C/min, and the morphological changes of the wax crystals, before and after addition of the additives, were observed at 200 × magnification.

2.10. X-ray diffraction

The structural characteristics of waxy model oil at 15 °C, both undoped and doped with PPDs, were analyzed using wide-angle X-ray diffraction (XRD). Experiments were performed on a Rigaku Ultima IV multi-crystal diffractometer (Japan) equipped with a copper target X-ray source (λ = 1.5406 Å). The measurement conditions were operating voltage of 35 kV, operating current of 25 mA, 2θ scanning range from 5° to 75°, step size of 0.02°, and scanning speed of 5° min^{-1}.

3. Results and discussion

3.1. FTIR analysis

Fig. 6 presents the FTIR spectra of EVA, EVAL, and EVAL-g-AAC polymer PPD materials. The characteristic absorption peak at 1741 cm^{-1} corresponds to both the ethylene chain and vinyl acetate moieties. The bending vibrational absorption of the –(C=O)O– group appears at 1252 cm^{-1} (Alves et al., 2023).

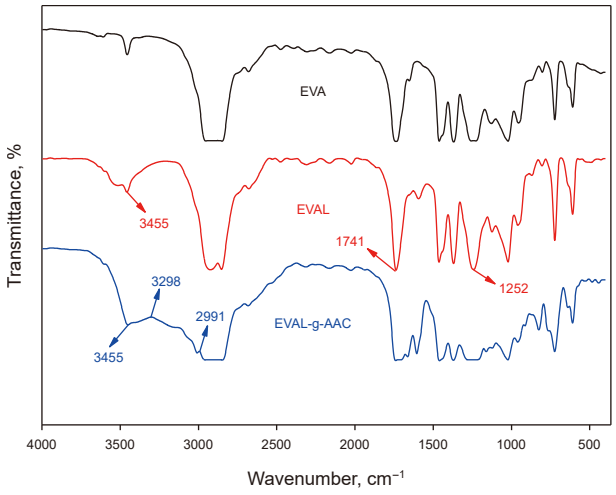

Fig. 6. FTIR spectra of EVA, EVAL, and EVAL-g-AAC.

Compared with EVA, the FTIR spectrum of EVAL exhibited a stronger –OH absorption peak at 3455 cm^{-1}, indicating the formation of free hydroxyl groups in its side chain. Meanwhile, the characteristic peaks at 1252 cm^{-1} and 1741 cm^{-1} were weakened, suggesting a reduction in carbonyl content and providing evidence for the successful preparation of EVAL. In the FTIR spectrum of EVAL-g-AAC, the –OH peak at 3455 cm^{-1} was diminished due to the esterification grafting of EVAL with AAC. A new peak at 3298 cm^{-1} corresponded to –OH stretching on the benzene ring, while the peak at 2991 cm^{-1} was attributed to =C–H stretching of the aryl ring. These features confirmed the presence of aromatic structures from anacardic acid in the product (Alaka et al., 2024; Philip et al., 2008) and demonstrated the successful grafting of anacardic acid onto the EVAL molecule.

3.2. ^{1}H NMR analysis

The ^{1}H NMR spectra of EVA, EVAL, and EVAL-g-AAC PPDs are presented in Fig. 7(a)–(c), respectively. From Fig. 7(a), the area ratio of the proton signal in the vinyl acetate group (f1 = 2.02 ppm) to that in the vinyl group (f1 = 1.24 ppm) was calculated according to Eq. (1), yielding a vinyl acetate content of 32.2 wt% for EVA, which is in good agreement with the nominal value of 32.0 wt%.

$$VA\ content = 3 \times Integral\ area\ of\ vinyl\ acetate\ H\ peak / integral\ area\ of\ vinyl\ H\ peak \quad (1)$$

Comparison of Fig. 7(a) and (b) shows the appearance of hydroxyl proton signals at f1 = 3.53 ppm and f1 = 3.67 ppm in EVAL. The area ratio of the vinyl acetate proton signal (f1 = 2.02 ppm) to that of the hydroxyl group (f1 = 4.84 ppm) decreased from 3.55 in EVA (Fig. 7(a)) to 3.36 in EVAL (Fig. 7(b)). These changes indicate that the ester groups of EVA were converted to hydroxyl groups, providing further evidence for the successful alcoholysis reaction (Ren et al., 2017).

The ^{1}H NMR spectrum of EVAL-g-AAC is presented in Fig. 7(c). Compared with Fig. 7(b), new peaks at f1 = 2.78 ppm and f1 = 2.96 ppm correspond to methylene protons in the alkyl chains attached to the aryl ring, while the peak at f1 = 5.02 ppm corresponds to the hydroxyl proton on the aryl ring of anacardic acid. Signals appearing between f1 = 6.23–5.06 ppm are attributed to allylic protons attached to the mono-, di-, and triene double bonds in the alkyl chain of the aryl ring (Alaka et al., 2024; Koteich Khatib et al., 2020). Together with the FTIR data, these results confirm the successful esterification of anacardic acid with EVAL, providing evidence for polymer grafting.

3.3. Contact angle analysis of deionized water

As shown in Fig. 8, the physical appearances of EVA, EVAL, and EVAL-g-AAC 2, along with their corresponding water contact angle measurements, are presented. Water contact angle tests indicate the material's polarity. The measured contact angles for EVA, EVAL, and EVAL-g-AAC 2 are 76.0°, 69.1°, and 52.9°, respectively. According to the principle of similarity and solubility, these results demonstrate that EVAL-g-AAC 2 exhibits stronger polarity than EVAL, consistent with the findings from structural characterization.

3.4. Pour point measurement

The initial pour point of the model oil, without any added PPDs, is 35 °C. As shown in Fig. 9(a), the extent of pour point reduction was compared for different PPDs at their optimal dosages. The model oil exhibited the greatest pour point reduction when 400 mg/kg of EVAL-g-AAC 2 was added, indicating superior

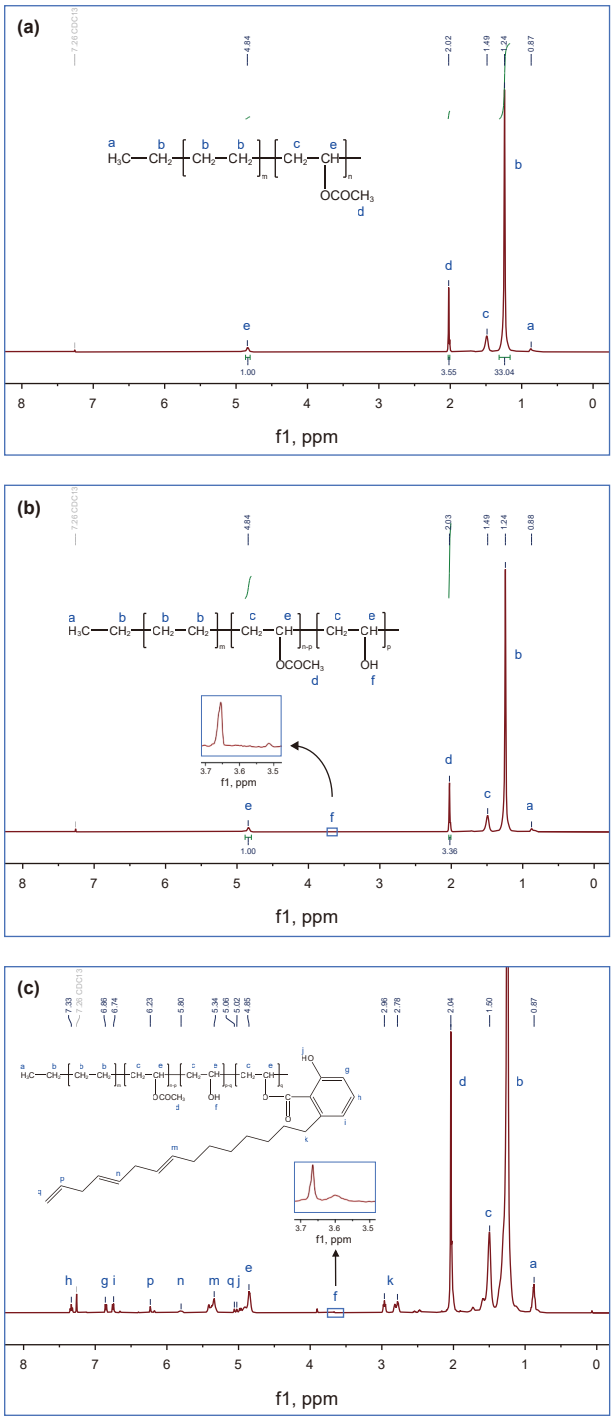

Fig. 7. ^{1}H NMR spectra of EVA (**a**), EVAL (**b**), and EVAL-g-AAC (**c**).

performance. This effect is attributed to its more effective interaction with wax crystals (as shown in Supplementary Fig. S1). Therefore, EVAL-g-AAC 2 was selected as the primary focus of this study. As shown in Fig. 9(b), at an additive concentration of 400 mg/kg, EVAL-g-AAC 2 reduces the pour point of the model oil by 24 °C. This improvement occurs because the pour point depressant provides attachment sites for wax crystals in the waxy model oil, thereby altering their growth direction and morphology. Excessive addition of the pour point depressant, however, can reduce intermolecular cohesion and hinder the formation of co-crystallization surfaces with wax crystals. Compared with model oils doped with the same amounts of EVA or EVAL, the addition of EVAL-g-AAC 2 further lowered the pour point by 8 °C and 5 °C, respectively, demonstrating its superior effectiveness in improving the low-temperature fluidity of waxy model oil.

3.5. Rheological properties analysis

3.5.1. Viscosity-temperature curves analysis

The viscosity-temperature curves of model oils, both undoped and doped with varying concentrations of EVAL-g-AAC 2, are presented in Fig. 10(a). Fig. 10(b) compares the viscosity-temperature profiles of model oils containing EVAL-g-AAC 2 with those containing EVA and EVAL at their respective optimal additive levels. In all cases, viscosity increased as temperature decreased due to aggregation and cross-linking of wax crystal molecules, which reduced the low-temperature fluidity of the model oils. Notably, the viscosity of the undoped model oil reached 631.9 mPa s at 15 °C. It was also observed that at an optimal dosage of 400 mg/kg, EVA reduced the viscosity of the model oil at 15 °C to 296.9 mPa s. This effect is likely due to co-crystallization between EVA polymer chains and wax crystal molecules, which alters the growth direction of wax crystals, weakens the low-temperature network structure, facilitates the flow of liquid oil, and thereby reduces viscosity (Xia et al., 2022b, 2024). For the model oil doped with EVAL, viscosity was further reduced to 272.4 mPa s, indicating that the introduction of polar −OH groups into EVA molecules enhances the dispersion of wax crystals and further lowers the viscosity of waxy model oil. In the case of 400 mg/kg EVAL-g-AAC 2, the viscosity at 15 °C decreased to 194.7 mPa s, and the onset of significant viscosity increase was delayed, corresponding to a viscosity reduction of 69.2%. This improvement is attributed to the modification of wax crystallization behavior: the co-crystallization of nonpolar groups with wax crystals, combined with the dispersive effect of polar groups, disrupts the cross-linked network of wax crystals. Nevertheless, at lower temperatures, extensive wax crystallization results in overlapping and cross-linking of wax crystals, causing a slight increase in viscosity.

3.5.2. Variable shear viscosity curves analysis

As shown in Fig. 11(a), the variable shear viscosity curves of model oils containing different dosages of EVAL-g-AAC 2 at 15 °C are presented, whereas Fig. 11(b) compares the curves obtained when EVA, EVAL, and EVAL-g-AAC 2 are each added at their respective optimal dosages. At low shear rates, strong intermolecular interactions within the model oil lead to relatively high viscosity. As the shear rate increases, these interactions are progressively disrupted, enabling easier molecular slippage and consequently reducing the viscosity. The pour point of the undoped model oil is 35 °C, and its viscosity gradually decreases with increasing shear rate. For model oils containing 400 mg/kg of EVA or EVAL, the apparent viscosity at a fixed shear rate of 200 s^{-1} decreases from 0.20 to 0.15 and 0.10 Pa s, respectively. This suggests that EVA molecules can hinder the stacking of wax crystals through a co-crystallization mechanism, thereby disrupting the gel-like network structure that forms at low temperatures under shear and ultimately reducing the viscosity (Xia et al., 2022b, 2024). EVAL molecules, derived from EVA through the introduction of polar groups, exhibit enhanced dispersion of wax crystals and therefore show lower apparent viscosity at the same shear rate. Compared with EVA and EVAL, EVAL-g-AAC 2 further reduces the apparent viscosity of the model oil to 0.06 Pa s. This superior performance is attributed to its higher polarity, which strengthens its ability to disperse wax crystals. In addition, the benzene ring structure of anacardic acid may promote heterogeneous nucleation with wax crystals, while its long alkyl chains can co-

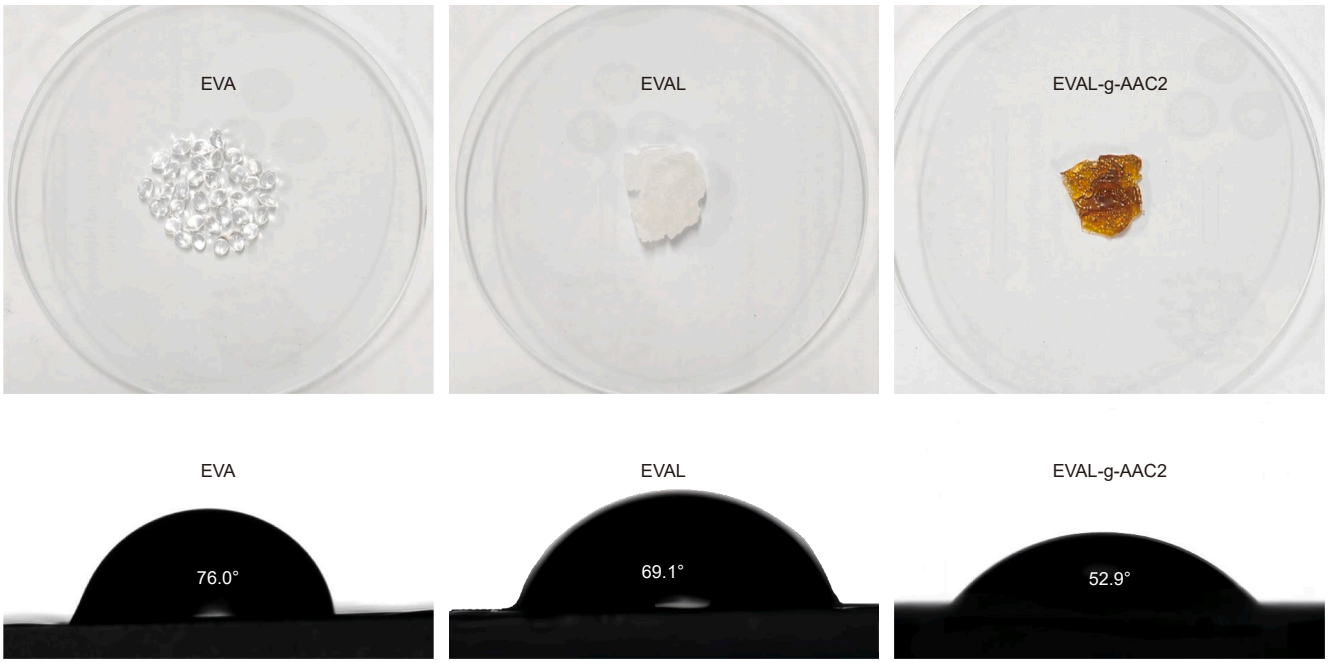

Fig. 8. Contact angle of deionized water for EVA, EVAL, and EVAL-g-AAC2.

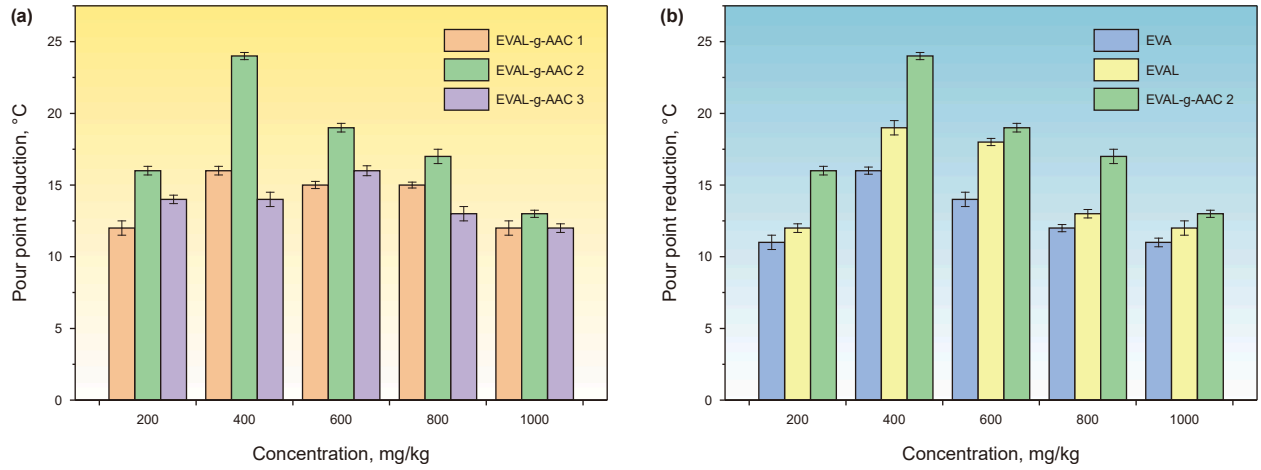

Fig. 9. Reduction of pour point of waxy model oils by different EVAL-g-AAC **(a)** and EVA, EVAL, and EVAL-g-AAC 2 **(b)**.

crystallize with wax molecules. Together, these interactions effectively modify wax crystallization behavior and further improve the rheological properties of the model oil.

3.5.3. Viscoelastic property curves analysis

As shown in Fig. 12, the gelation temperature of the waxy model oil is 40.2 °C. When the temperature falls below this point, the storage modulus (G′) begins to exceed the loss modulus (G″). With further cooling, the elastic response becomes dominant, and the system transitions into a gel-like state. After the addition of EVA, the gelation temperature increases slightly, and both G′ and G″ at low temperatures are marginally lower than those of the undoped model oil. When EVAL is introduced, the gelation temperature rises to 41.6 °C, and the corresponding G′ and G″ values at 15 °C reach 38,683 and 6565 Pa, respectively. Compared with EVA and EVAL, the incorporation of EVAL-g-AAC 2 reduced the gelation temperature of the model oil to 39.7 °C, and the corresponding G′ and G″ values at 15 °C decreased to 6606 and 2189 Pa, respectively. This indicates that the addition of EVAL-g-AAC 2 suppresses the formation of the gel structure in the waxy model oil and weakens its viscoelasticity under low-temperature conditions, as reflected by the reduced G′ and G″ values accompanying wax crystallization. Because the viscoelastic behavior of waxy model oil is closely related to both the morphology and quantity of precipitated wax crystals, the microstructural observations in Fig. 15(c) further support this conclusion. The incorporation of EVAL-g-AAC 2 disrupts the three-dimensional network formed by wax crystals, creating more space for liquid oil to flow. Consequently, the viscoelastic properties of the oil sample are diminished, leading to the observed decreases in G′ and G″.

3.5.4. Yield property curves analysis

As shown in Fig. 13(a), the variation curves of shear stress versus shear strain at 15 °C for the waxy model oils undoped/doped with different additions of EVAL-g-AAC 2, and Fig. 13(b), the variation curves of shear stress versus shear strain at 15 °C for the waxy model oils doped with 400 mg/kg of EVA, EVAL and EVAL-g-AAC 2,

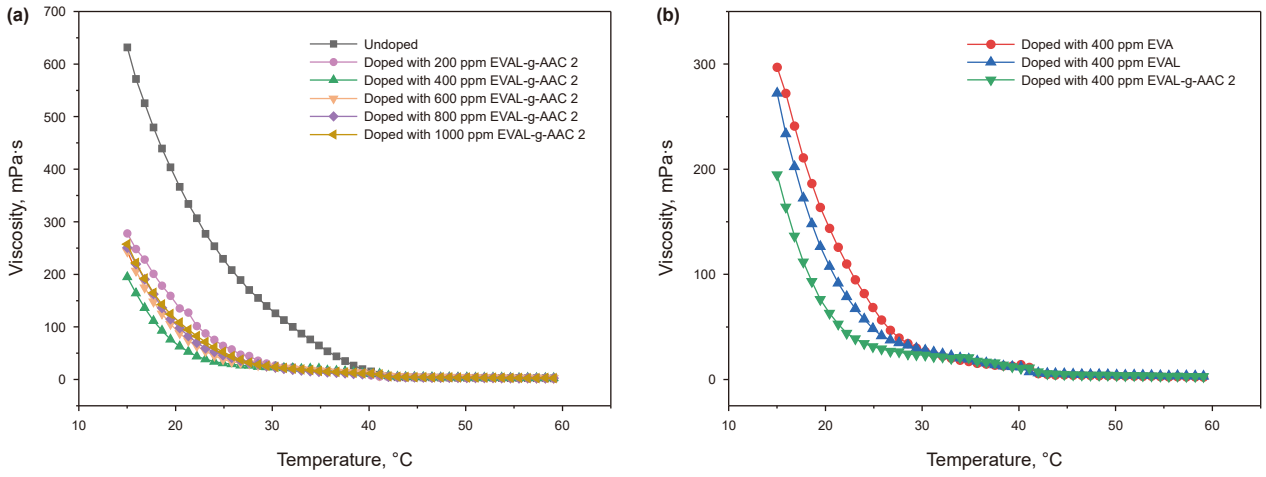

Fig. 10. Viscosity-temperature curves of oil samples: **(a)** undoped and doped with different concentrations of EVAL-g-AAC 2; **(b)** doped with 400 mg/kg PPDs.

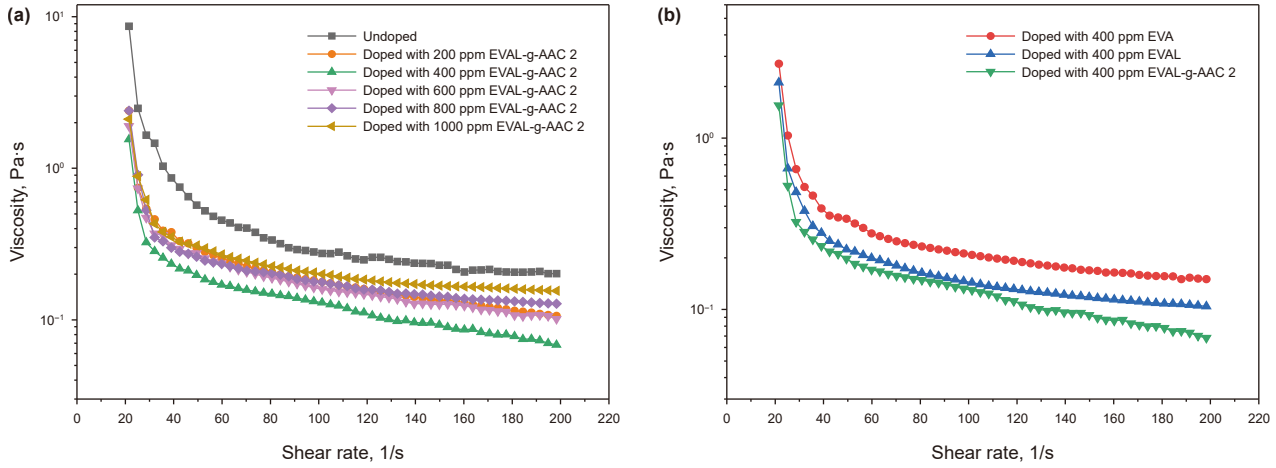

Fig. 11. Variable shear viscosity curves of oil samples: **(a)** undoped and doped with different concentrations of EVAL-g-AAC 2; **(b)** doped with 400 mg/kg PPDs.

respectively. It can be observed that the yield stress of the model oil without PPD doping is 73.43 Pa at a strain of 6×10^6, the yield stress of the model oil with 400 mg/kg of EVA PPD at a strain of 6×10^6 is 15.74 Pa, and the yield value of the same concentration of EVAL was 13.75 Pa, which was 12.64% lower than that of pure EVA agent. This indicates that, compared with conventional EVA, the introduction of polar groups can better inhibit the formation and strength of the gel structure of waxy model oil (Xia et al., 2022b, 2024). Compared with EVA and EVAL, the model oil containing 400 mg/kg EVAL-g-AAC 2 exhibited a yield stress of 9.50 Pa at the same strain, representing reductions of 30.91% relative to EVAL and 87.06% relative to the original waxy model oil. These results indicate that the incorporation of EVAL-g-AAC 2 not only weakens the gel structure of the model oil at a given temperature, but also further decreases the shear stress as shear strain increases. Such improvements are beneficial for crude oil transportation and pipeline restart operations. Therefore, EVAL-g-AAC 2 shows significant potential for optimizing and managing crude oil pipeline transportation and storage systems, highlighting its prospective commercial value.

3.6. Analysis of X-ray diffraction

The crystal structures of wax crystals in the model oil were analyzed using X-ray diffraction (XRD). As shown in Fig. 14, the XRD patterns of the undoped model oil and the samples doped with different PPDs are compared. After the addition of PPDs, new diffraction peaks appear at $2\theta \approx 30°$ and 36.1°. These newly emerged peaks are presumed to result from the formation of additional crystal planes, likely induced by hydrogen bonding or van der Waals interactions between the wax crystals and the PPDs (Huang et al., 2018; Zhang, 2003). The diffraction peaks at $2\theta \approx 6.1°$, 21.5°, and 23.9° correspond to the (006), (110), and (200) crystal planes, respectively. Upon addition of PPDs, the intensity of the (006) peak decreases, whereas the intensities of the (110) and (200) peaks increase. The absence of peak shifts for the (110) and (200) planes indicates that the orthorhombic crystal structure of the wax crystals remains unchanged (Guin and Naiya, 2025; Yan et al., 2025). It can also be observed that the intensities of the diffraction peaks at these two positions increase progressively with the addition of EVA, EVAL, and EVAL-g-AAC 2. This variation reflects changes in crystallization integrity, which can be quantified using the crystallinity index (CI). The CI is calculated using Eq. (2), where h, k, and l denote the Miller indices of the wax crystal, A represents the area of the diffraction peak, and m is the number of diffraction peaks (Huang et al., 2018).

$$\mathrm{CI} = \sum_{i=1}^{m} A_{hkl} / A_{\text{Total diffraction intensity}} \times 100\% \quad (2)$$

The crystallinity index (CI) of the undoped model oil is 17.39%. Upon addition of PPDs, the CI values increase to 34.16%

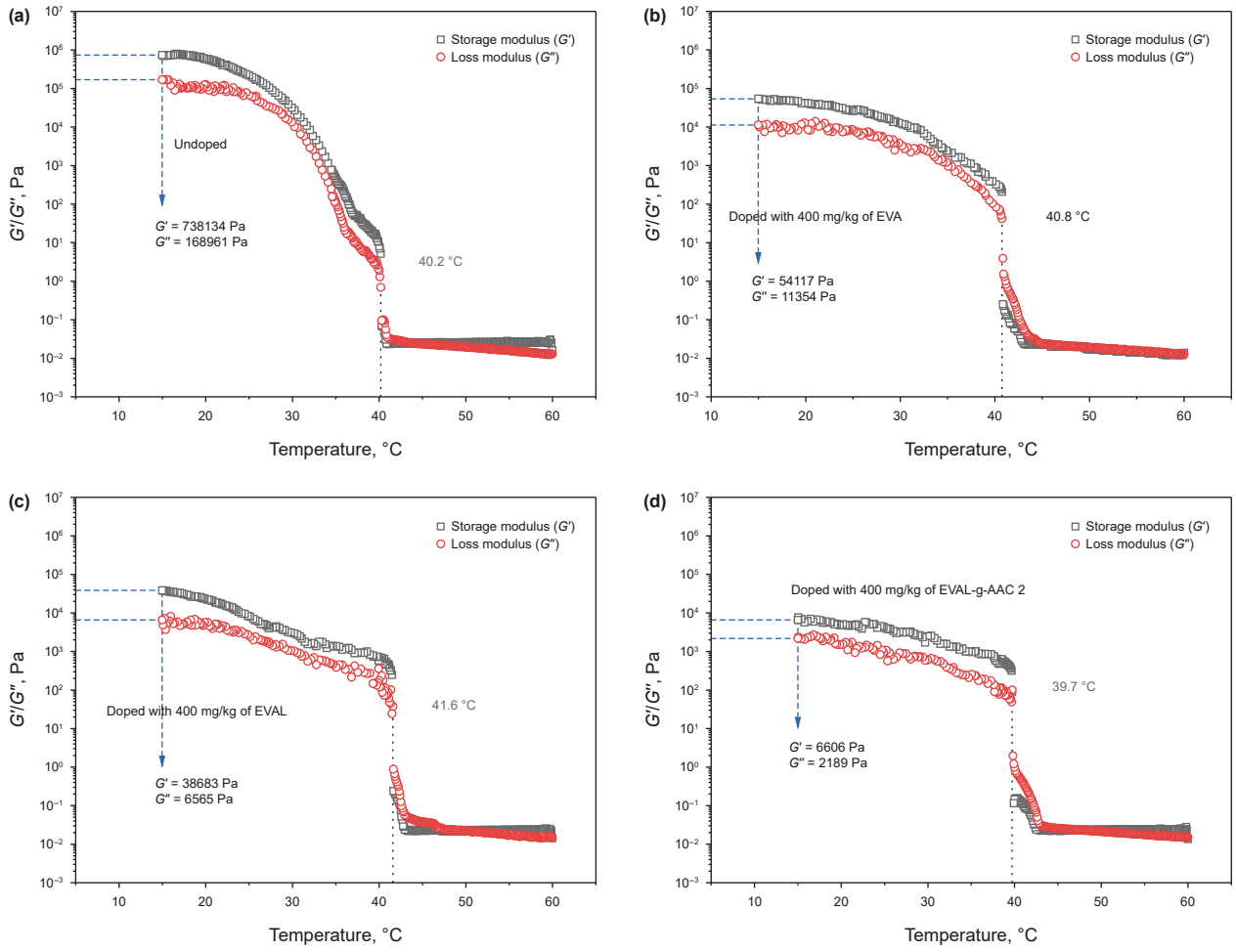

Fig. 12. Viscoelastic behavior curves of undoped waxy model oil **(a)** and model oils doped with 400 mg/kg of EVA **(b)**, EVAL **(c)**, and EVAL-g-AAC 2 **(d)**.

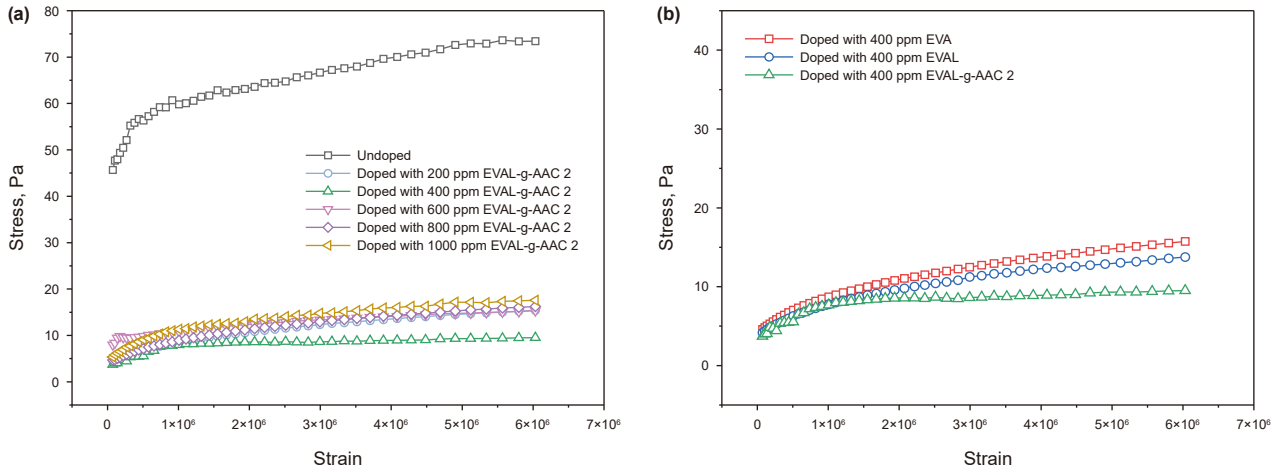

Fig. 13. Yield property curves of oil samples: **(a)** undoped and doped with different concentrations of EVAL-g-AAC 2; **(b)** doped with 400 mg/kg PPDs.

for EVA, 32.52% for EVAL, and 30.88% for EVAL-g-AAC 2. This increase is attributed to the ability of polymeric PPDs to interfere with the crystallization of waxes, promoting the formation of partially amorphous wax structures (Soliman et al., 2018). Notably, the introduction of nonpolar alkyl long chains in EVAL-g-AAC 2 enhances co-crystallization with wax crystals, effectively inhibiting their growth along the *x*- and *z*-axes. This reduces the interplanar spacing and promotes the orderly stacking of wax crystals in a specific orientation, ultimately leading to an increase in the intensity of the diffraction peaks corresponding to the (110) and (200) crystal planes (Soliman et al., 2018; Sun et al., 2024b).

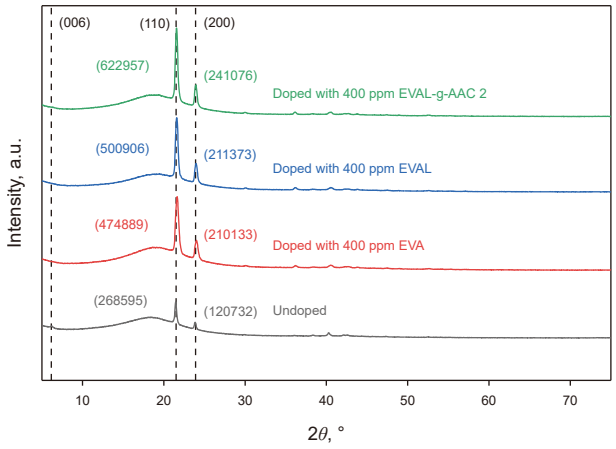

Fig. 14. XRD spectrum of waxy model oil, undoped/doped with PPDs at 15 °C.

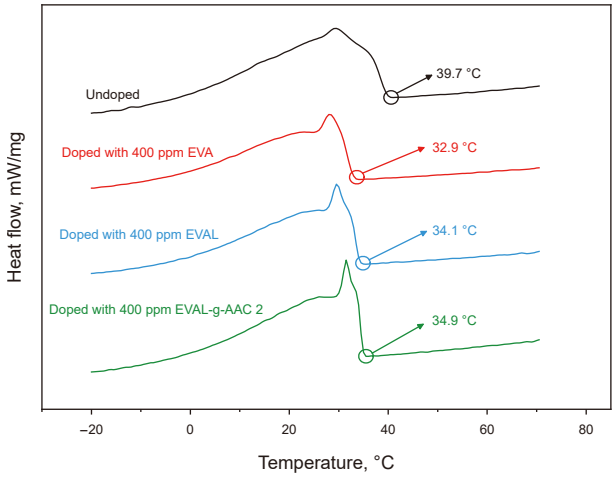

Fig. 15. DSC of waxy model oils, undoped and doped with different PPDs.

3.7. DSC analysis

Fig. 15 presents the DSC curves of the waxy model oil without a pour point depressant and with EVA, EVAL, and EVAL-g-AAC 2 during the cooling process. The exothermic peak of the undoped model oil, appearing at 39.7 °C, corresponds to the crystallization of waxes. The addition of EVA, EVAL, and EVAL-g-AAC 2 all reduced the wax crystallization temperature. Notably, the wax precipitation temperature in EVA-doped model oil decreased by approximately 7 °C, which can be attributed to the PPD promoting higher supercooling in the waxy crude oil and thus lowering the wax appearance temperature (WAT). Additionally, the DSC curves of PPD-doped model oils exhibit sharper exothermic peaks, indicating more defined crystallization events. This rapid crystallization is expected in waxy model oil with higher supersaturation. For EVAL, the resins and asphaltene molecules in the waxy model oil contain numerous amino and hydroxyl groups, allowing EVAL to readily form hydrogen bonds with them. This interaction produces EVAL-resin-asphaltene aggregates, which act as additional nucleation sites for wax crystals, participating in their formation and partially promoting wax precipitation. Consequently, the wax appearance temperature (WAT) of the model oil containing EVAL is 1.2 °C higher than that of the model oil containing EVA (Ren et al., 2017). The EVAL-g-AAC 2 pour point depressant is derived from EVAL with hydroxyl groups and incorporates the molecular structure of anacardic acid. The hydroxyl groups on the aromatic ring of anacardic acid further increase the polarity of the depressant molecule, facilitating the dispersion of wax crystals in the model oil (Yang et al., 2021). However, the increased polarity of the polymer molecule slightly reduces its solubility in the oil phase. Simultaneously, the introduction of rigid benzene rings into the molecular structure of the pour point depressant enhances its promotion of wax crystal nucleation (Huang et al., 2018; Lin et al., 2020; Yin et al., 2020), leading to a slight increase in the wax appearance temperature (WAT) of the EVAL-g-AAC 2-doped model oil compared with the EVAL-doped model oil.

3.8. Micro-observation of the undoped/doped waxy model oil

As shown in Fig. 16, the microscopic morphology of wax crystals in undoped and PPD-doped model oils was observed at 15 °C. In Fig. 16(b), the model oil doped with EVA exhibits improved wax crystal dispersion, disrupting the three-dimensional network structure of the wax crystals. In Fig. 16(c), the model oil doped with EVAL shows larger but sparser wax crystals. This effect is attributed to the hydroxyl groups in EVAL, which increase the polarity of the polymer, enhance the dispersion of wax crystals, and inhibit their agglomerative cross-linking. Binarized POM images and quantitative analyses are presented in Supplementary Fig. S3. As shown in Fig. 16(d), the wax crystals in the model oil doped with EVAL-g-AAC 2 are more sparsely distributed, indicating a stronger dispersion effect. This behavior can be attributed to multiple factors: the benzene ring in EVAL-g-AAC 2, acting as a rigid structure, promotes wax crystal nucleation (Lin et al., 2020; Yin et al., 2020); the long alkyl chains on the benzene ring enhance co-crystallization with wax crystal molecules (Cui et al., 2024); and the hydroxyl groups inherent to the benzene ring in anacardic acid increase the polarity of EVAL-g-AAC 2, further improving the dispersion of wax crystals.

3.9. Discussion on the mechanism of EVAL-g-AAC 2 PPD

As shown in Fig. 17, the contact angle measurements of deionized water, combined with DSC analysis, indicate that the increased polar groups in EVAL-g-AAC 2 promote the dispersion of wax crystals, leading to a more uniform and sparse distribution (Yang et al., 2020, 2021). Furthermore, XRD analysis reveals that the introduction of non-polar alkyl long chains enhances the co-crystallization with wax crystals and effectively directs their growth orientation (Pucko et al., 2022; Zhang et al., 2022). At the same time, combining the microscopic images of wax crystals in Fig. 15, it can be inferred that the aromatic ring in the EVAL-g-AAC 2 molecule, acting as a rigid structure, serves as a nucleation site for wax crystals. This rigid structure functions as a precipitation template, promoting wax crystal nucleation and altering their growth habits (Lin et al., 2020; Yin et al., 2020). It can be concluded that EVAL-g-AAC 2, a novel pour point depressant, operates via a threefold synergistic mechanism that improves the crystallization behavior of wax molecules: “alkyl long chains promote co-crystallization, polar groups enhance dispersion, and rigid structures facilitate nucleation.” Moreover, the synergistic interaction between the polar benzene ring and the nonpolar long-chain groups alters the morphology of the wax crystals, contributing to improved low-temperature flow properties of the model oil (Wang et al., 2024). Interactions between polar molecules slow the precipitation of wax crystals, resulting in larger crystal sizes that reduce the solid-liquid interfacial area. This hinders the formation of the gel network structure, thereby enhancing the low-temperature mobility of waxy model oils.

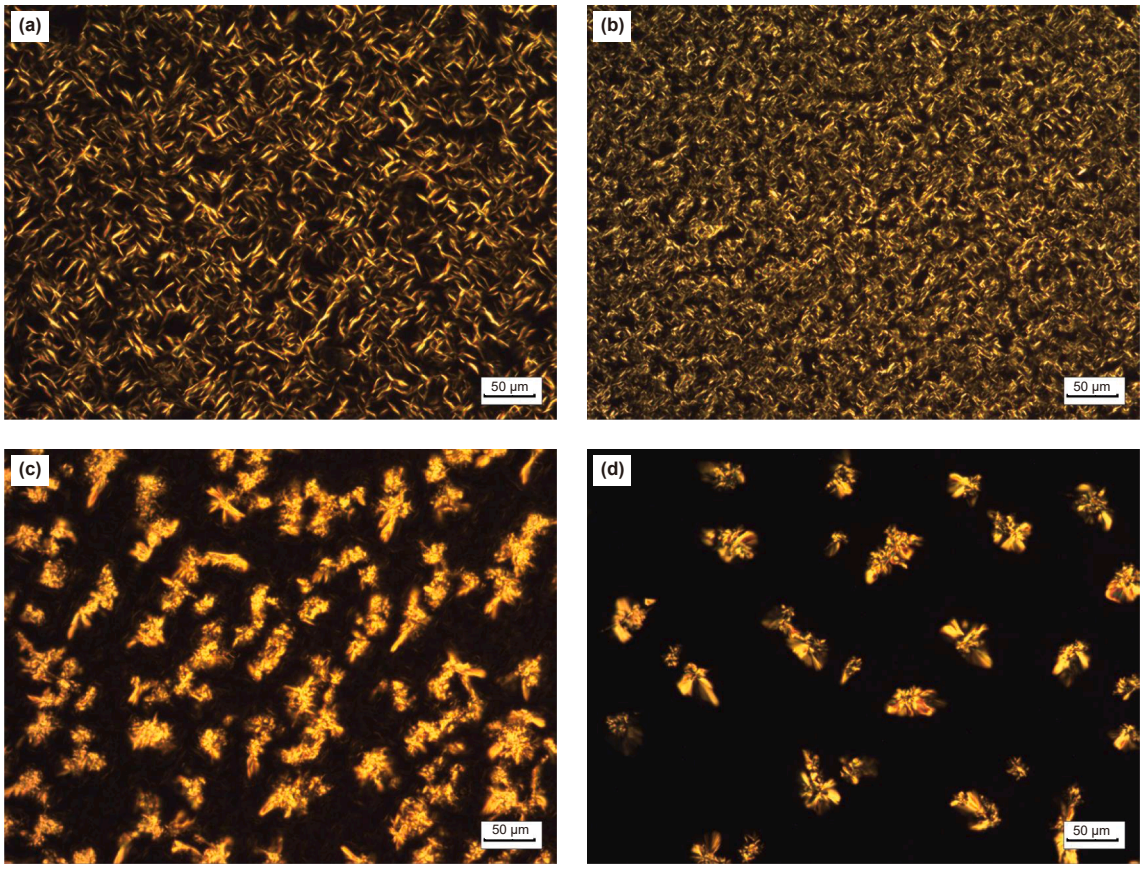

Fig. 16. Microscopic images of waxy model oil with undoped and doped with PPDs at 15 °C: **(a)** undoped; doped with **(b)** 400 mg/kg EVA;**(c)** 400 mg/kg EVAL; **(d)** 400 mg/kg EVAL-g-AAC 2.

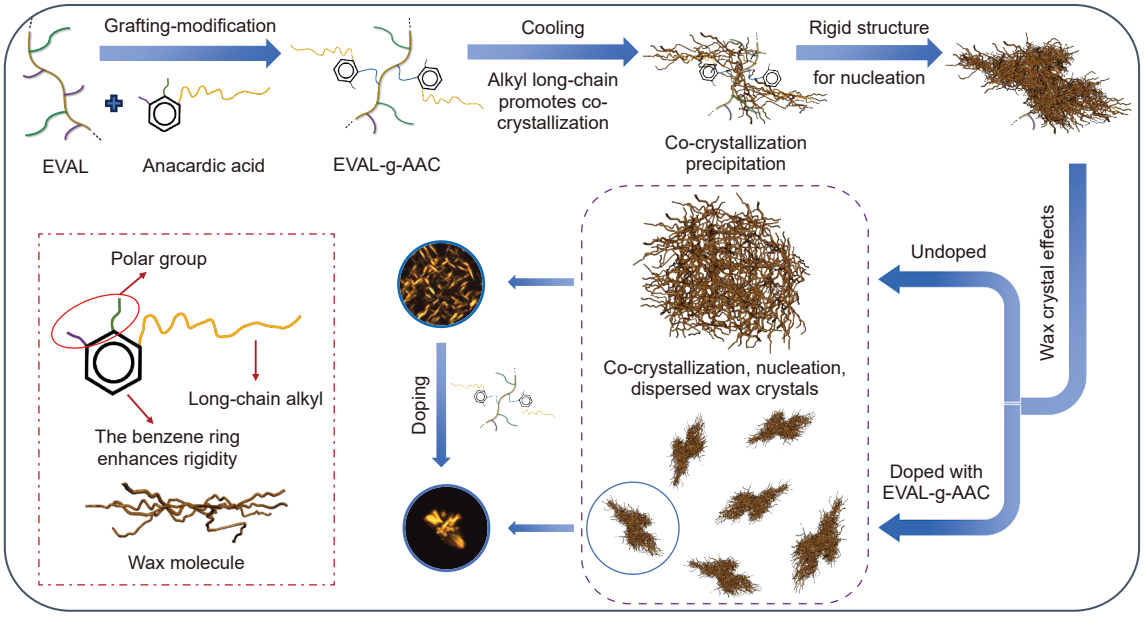

Fig. 17. Possible mechanism of EVAL-g-AAC 2 novel PPD to improve the low-temperature flowability of waxy model oil.

4. Conclusion

In this study, EVAL was obtained via alcoholysis of EVA, and CNSL, a cashew nut shell liquid rich in anacardic acid, was extracted from cashew nut shells using a low-boiling polar solvent. Subsequently, the anacardic acid in CNSL was used to chemically graft and modify EVAL, yielding three novel PPDs with EVAL-to-CNSL mass ratios of 1:1, 1:2, and 1:3. The optimal EVAL-g-AAC

formulation was determined through comparative analysis of pour point reduction and wax crystal morphology. EVA, EVAL, and the optimized EVAL-g-AAC were further characterized using ^{1}H NMR spectroscopy, Fourier-transform infrared spectroscopy, and rheological testing on waxy model oils. The results indicate that this novel PPD, acting as a template for wax crystal precipitation, effectively enhances the low-temperature rheological properties of waxy model oils and disrupts the gel network formed under low-temperature conditions by altering the growth direction of wax crystals. It also exhibits strong co-crystallization and dispersion effects on wax crystal aggregates. Anacardic acid, as an inexpensive and readily available biomass resource, provides a promising strategy for developing low-cost, high-efficiency crude oil PPDs through graft modification with conventional polymer-based PPDs.

CRediT authorship contribution statement

Zheng-Nan Sun: Methodology. **Pei-Song Shi:** Writing – original draft, Resources, Formal analysis, Data curation. **Yi-Hai Yang:** Validation. **Ming-Xing Bai:** Funding acquisition. **Guo-Lin Jing:** Methodology. **Cai-Yu Guan:** Supervision.

Declaration of competing interest

The authors declare that they have no known competing financial interests or personal relationships that could have appeared to influence the work reported in this paper.

Acknowledgments

This work was supported by Hebei Natural Science Foundation (Grant No. E2025107002).

Appendix A. Supplementary data

Supplementary data to this article can be found online at https://doi.org/10.1016/j.petsci.2026.01.017.

References

Alaka, M.O., Ogunjobi, J.K., Oluwasina, O.O., Lajide, L., 2024. Studies on Nigerian cashew nut shell liquid: Greening-up extraction process, chemical composition and cost effectiveness. Sustain. Chem. Environ. 7, 100139. https://doi.org/10.1016/j.scenv.2024.100139.

Alves, B.F., Silva, B.K.M., Silva, C.A., Celestino, G.G., Nunes, R.C.P., Lucas, E.F., 2023. Preparation and evaluation of polymeric nanocomposites based on EVA/montmorillonite, EVA/palygorskite and EVA/halloysite as pour point depressants and flow improvers of waxy systems. Fuel 333, 126540. https://doi.org/10.1016/j.fuel.2022.126540.

Anghelache, C., Anghel, M.G., Iacob, Ştefan V., Pârțachi, I., Rădulescu, I.G., Brezoi, A.G., 2023. Analysis of the situation of renewable and non-renewable energy consumption in the European union. Energies 16, 1338. https://doi.org/10.3390/en16031338.

Cui, L.L., Li, X., Ren, F.H., Lin, H.L., Han, S., 2024. A novel pour point depressant with diesel cold-flow properties: Performance evaluation of benzene-containing ternary copolymers. Energy 288, 129607. https://doi.org/10.1016/j.energy.2023.129607.

Dengaev, A.V., Kayumov, A.A., Getalov, A.A., Aliev, F.A., Baimukhametov, G.F., Sargin, B.V., Maksimenko, A.F., Vakhin, A.V., 2023. Chemical viscosity reduction of heavy oil by multi-frequency ultrasonic waves with the main harmonics of 20–60 kHz. Fluids 8, 136. https://doi.org/10.3390/fluids8040136.

Du, Y.N., Huang, C., Jiang, W., Yan, Q.W., Li, Y.F., Chen, G., 2024. Preparation of surface modified nano-hydrotalcite and its application as a flow improver for crude oil. Fuel 357, 130005. https://doi.org/10.1016/j.fuel.2023.130005.

Eke, W.I., Kyei, S.K., Achugasim, O., Ajienka, J.A., Akaranta, O., 2024. Formulation and application of cashew nutshell liquid derivatives as potential oilfield chemical for crude oil flow assurance. Biomass Convers. Biorefinery 14, 11131–11144. https://doi.org/10.1007/s13399-022-03215-4.

Eke, W.I., Kyei, S.K., Ajienka, J., Akaranta, O., 2021. Effect of bio-based flow improver on the microscopic and low-temperature flow properties of waxy crude oil. J. Pet. Explor. Prod. Technol. 11, 711–724. https://doi.org/10.1007/s13202-020-01078-x.

Gandhi, T.S., Dholakiya, B.Z., Patel, M.R., 2013. Extraction protocol for isolation of CNSL by using protic and aprotic solvents from cashew nut and study of their physico-chemical parameter. Pol. J. Chem. Technol. 15 (4), 24–27. https://doi.org/10.2478/pjct-2013-0062.

Guin, S., Naiya, T.K., 2025. Enhancement of cold flowability of waxy crude oil using eco-friendly PPDs synthesized from stearic acid and lauric acid – experimental, modelling, and mechanistic approach. J. Mol. Liq. 426, 127363. https://doi.org/10.1016/j.molliq.2025.127363.

Huang, H.R., Wang, W., Peng, Z.H., Ding, Y.F., Li, K., Li, Q.P., Gong, J., 2018. The influence of nanocomposite pour point depressant on the crystallization of waxy oil. Fuel 221, 257–268. https://doi.org/10.1016/j.fuel.2018.01.040.

Khatri, S.A., Mirjat, N.H., Harijan, K., Uqaili, M.A., Shah, S.F., Shaikh, P.H., Kumar, L., 2022. An overview of the current energy situation of Pakistan and the way forward towards green energy implementation. Energies 16, 423. https://doi.org/10.3390/en16010423.

Koteich Khatib, S., Bullón, J., Vivas, J., Bahsas, A., Rosales-Oballos, Y., Marquez, R., Forgiarini, A., Salager, J.L., 2020. Synthesis, characterization, evaluation of interfacial properties and antibacterial activities of dicarboxylate anacardic acid derivatives from cashew nut shell liquid of *Anacardium occidentale* L. J. Surfactants Deterg. 23, 503–512. https://doi.org/10.1002/jsde.12384.

Kuzmin, K.A., Kosolapova, S.M., Rudko, V.A., 2024. Investigating the mechanism of action of polymer pour point depressants on cold flow properties of biodiesel fuels. Colloids Surf. A Physicochem. Eng. Asp. 702, 134971. https://doi.org/10.1016/j.colsurfa.2024.134971.

Kuzmin, K.A., Sultanbekov, R.R., Khromova, S.M., Vovk, M.A., Rudko, V.A., 2025. Establishing the influence of recycled used oil on the sedimentation stability of residual marine fuel. Fuel 389, 134625. https://doi.org/10.1016/j.fuel.2025.134625.

Li, B.F., Guo, Z.Y., Du, M.J., Han, D.Y., Han, J., Zheng, L.M., Yang, C., 2024a. Research status and outlook of mechanism, characterization, performance evaluation, and type of pour point depressants in waxy crude oil: A review. Energy Fuel. 38, 7480–7509. https://doi.org/10.1021/acs.energyfuels.3c04555.

Li, B.F., Guo, Z.Y., Zheng, L.M., Shi, E.X., Qi, B., 2024b. A comprehensive review of wax deposition in crude oil systems: Mechanisms, influencing factors, prediction and inhibition techniques. Fuel 357, 129676. https://doi.org/10.1016/j.fuel.2023.129676.

Lin, H.L., Xie, M.Y., Yin, S.Y., Yang, T.S., Su, B.T., Chen, F.F., Han, S., Xue, Y., 2020. Influence of methacrylate-benzyl methacrylate-N-vinyl-2-pyrrolidone as pour point depression on cold flow properties of diesel fuel. Energy Fuel. 34, 1514–1523. https://doi.org/10.1021/acs.energyfuels.9b03603.

Liu, W.C., Huang, Q.Y., Chen, J.J., Jiang, C.J., Huang, R.Y., Zheng, H.P., 2025. Analysis of pipeline clogging by oil sticking during low-temperature transportation using XDLVO theory. Energy 320, 135160. https://doi.org/10.1016/j.energy.2025.135160.

Liu, Y., Sun, Z.N., Jing, G.L., Liu, S., Yang, Y.H., Xu, J.Q., 2021. Synthesis of chemical grafting pour point depressant EVAL-GO and its effect on the rheological properties of Daqing crude oil. Fuel Process. Technol. 223, 107000. https://doi.org/10.1016/j.fuproc.2021.107000.

Liu, Y., Sun, Z.N., Ji, S.Z., Yang, Y.H., Xu, J.Q., Jing, G.L., 2023. Effect of nanocomposite pour point depressant EVAL/CNT on flow properties of waxy crude oil. Pet. Sci. 20, 3807–3818. https://doi.org/10.1016/j.petsci.2023.05.016.

Marenov, B.T., Nadirov, K.S., Zhantasov, M.K., Nadirov, R.K., 2020. Ethylene-vinyl acetate copolymer/crude gossypol compositions as pour point depressants for waxy oil. Int. J. Chem. Eng. 2020, 1–7. https://doi.org/10.1155/2020/4195382.

Modi, P., Nagar, A., 2024. Synthesis of terpolymer from helianthus annuus (natural oil) and evaluation as pour point depressant and viscosity reducer on Indian crude oil. J. Dispersion Sci. Technol. 45, 1039–1048. https://doi.org/10.1080/01932691.2024.2315484.

Muñoz, J.A.D., Ancheyta, J., 2024. Techno-economic study of the effect of different distillates and crude oil diluents on the transportation by pipeline of heavy crude oil. Ind. Eng. Chem. Res. 63, 2063–2072. https://doi.org/10.1021/acs.iecr.3c04316.

Pandian, S., Dahyalal, P.C., Krishna, S., Hari, S., Subramanian, D., 2021. A study on cashew nut shell liquid as a bio-based flow improver for heavy crude oil. J. Pet. Explor. Prod. Technol. 11, 2287–2297. https://doi.org/10.1007/s13202-021-01162-w.

Philip, J.Y.N., Da Cruz Francisco, J., Dey, E.S., Buchweishaija, J., Mkayula, L.L., Ye, L., 2008. Isolation of anacardic acid from natural Cashew Nut Shell Liquid (CNSL) using supercritical carbon dioxide. J. Agric. Food Chem. 56, 9350–9354. https://doi.org/10.1021/jf801532a.

Pucko, I., Racar, M., Faraguna, F., 2022. Synthesis, characterization, and performance of alkyl methacrylates and tert-butylaminoethyl methacrylate tetra polymers as pour point depressants for diesel influence of polymer composition and molecular weight. Fuel 324, 124821. https://doi.org/10.1016/j.fuel.2022.124821.

Ragab, A.A., Sayed, M.A., Yassin, F., Baghi, H., 2025. Synthesis, evaluation and characterization of vinyl acetate/octadecyl acrylate copolymer as an energy-saving liquid pour point depressant for waxy crude oil. J. Mol. Liq. 420, 126835. https://doi.org/10.1016/j.molliq.2024.126835.

Ren, Y.W., Chen, Z.J., Du, H., Fang, L., Zhang, X.D., 2017. Preparation and evaluation of modified ethylene–vinyl acetate copolymer as pour point depressant and flow improver for jianghan crude oil. Ind. Eng. Chem. Res. 56, 11161–11166. https://doi.org/10.1021/acs.iecr.7b02929.

Shittu, O.M., Achugasim, O., 2023. Modified and unmodified Jatropha curcas seed oils as pour point depressants for a Nigerian waxy crude oil. J. Appl. Sci. Environ. Manag. 27, 237–242. https://doi.org/10.4314/jasem.v27i2.8.

Soliman, E.A., Elkatory, M.R., Hashem, A.I., Ibrahim, H.S., 2018. Synthesis and performance of maleic anhydride copolymers with alkyl linoleate or tetra-esters as pour point depressants for waxy crude oil. Fuel 211, 535–547. https://doi.org/10.1016/j.fuel.2017.09.038.

Sultanbekov, R., Schipachev, A., 2022. Manifestation of incompatibility of marine residual fuels: a method for determining compatibility, studying composition of fuels and sediment. J. Min. Inst. Online first. https://doi.org/10.31897/PMI.2022.56.

Sun, X.S., Hou, L., Tang, S.S., Wang, M.C., Xiong, Y.F., Zhu, Z.L., 2024a2024. Removal mechanism of adhering heavy oil from pipeline wall in low-temperature flow. Energy 296, 131118. https://doi.org/10.1016/j.energy.2024.131118.

Sun, X.J., Jia, L.L., Li, X.Y., Zhang, S.R., Wang, Y.T., Fan, M.W., Xu, J., 2024b. Geometric confinement growth of wax crystals by star acrylate polymer for enhanced cold flowability of waxy crudes. Fuel 372, 132083. https://doi.org/10.1016/j.fuel.2024.132083.

Sun, Z.N., Li, H.J., Jing, G.L., Zhang, F.N., Yan, B., Liu, X.Y., 2023. Application of EVA and its modified polymer in crude oil pour point depressant field. Chem. Ind. Eng. Prog. 42, 2987. https://doi.org/10.16085/j.issn.1000-6613.2022-1445.

Uzoh, C.F., John, S.U., Ezea, H.A., Igbonekwu, L.I., Madiebo, E.M., 2025. The study of the effectiveness of soybean oil and castor oil as flow improvers for waxy petroleum crude oil. J. Pet. Explor. Prod. Technol. 15, 73. https://doi.org/10.1007/s13202-025-01969-x.

Wang, H.G., Zhang, X.K., Lei, X.W., Chen, L., Wang, S.Y., Lin, H.L., Han, S., 2024. Effects of comb-like poly-α-olefins on the cold flow properties of diesel fuel. Fuel 356, 129562. https://doi.org/10.1016/j.fuel.2023.129562.

Xia, X., Li, C.X., Dai, S.T., Duan, Z., Lian, W.L., Yao, B., Sun, G.Y., Yang, F., 2022a. Modification effect of macroporous comb-like polymeric pour point depressants on the flow behavior of model waxy oils. Fuel 314, 123113. https://doi.org/10.1016/j.fuel.2021.123113.

Xia, X., Li, C.X., Sun, G.Y., Zhao, K.K., Zhang, J., Yao, B., Yang, F., 2022b. Performance improvement of Ethylene−Vinyl Acetate Copolymer Pour Point Depressant (EVA PPD) by adding small dosages of Laurylamine (LA). Pet. Sci. 19, 2472–2482. https://doi.org/10.1016/j.petsci.2022.04.002.

Xia, X., Shi, H.M., Li, C.X., Li, X.Y., Sun, G.Y., Yao, B., Zhao, Y.S., Yang, F., 2024. Mechanistic study on the effect of molecular structure characteristics of asphaltene on the synergistic modification with EVA on model waxy oil. Energy Fuel. 38, 1836–1844. https://doi.org/10.1021/acs.energyfuels.3c04436.

Xie, Y.W., Li, H.Y., Liang, B., Li, Q.D., Su, Y., Zhang, C.Y., Kang, J.B., Yang, Z.M., Su, H., Ji, Z.L., Zhang, J.J., 2025. Performance and mechanism of a novel electromagnetic treatment for improving the cold flowability of waxy crude oil. Fuel 382, 133803. https://doi.org/10.1016/j.fuel.2024.133803.

Xu, B.W., Sun, B., Cui, L.L., Chen, J.H., Chen, X.M., Li, X.Y., Wang, Z.C., Han, S., Xue, Y., 2023. Evaluation of the star anise extract as a natural cold flow improver for enhancing the cold flow properties of diesel fuel. Renew. Energy 215, 119028. https://doi.org/10.1016/j.renene.2023.119028.

Xue, Y., Zhao, Z.C., Xu, G.W., Lian, X., Yang, C., Zhao, W.N., Ma, P., Lin, H.L., Han, S., 2016. Effect of poly-alpha-olefin pour point depressant on cold flow properties of waste cooking oil biodiesel blends. Fuel 184, 110–117. https://doi.org/10.1016/j.fuel.2016.07.006.

Yan, F., Huang, Z.M., Li, Q.F., Xu, S.B., Nie, C.F., Xia, X., Yang, F., 2024. Preparation and performance evaluation of a new type of polyethylene-vinyl acetate/polystyrene microsphere composite pour point depressant for waxy crude oil. ACS Omega 9, 30873–30883. https://doi.org/10.1021/acsomega.4c03728.

Yan, S.L., Li, X.Y., Zhang, J.J., Xiao, P., Niu, M.F., Pi, Y.F., Xu, J., 2025. Enhancement of cold flowability for high waxy crude oil by the mildly crosslinked poly(styrene-octadecyl acrylate). J. Dispersion Sci. Technol. 46, 784–795. https://doi.org/10.1080/01932691.2023.2301463.

Yang, F., Zhu, B.W., Li, C.X., Sun, G.Y., Wang, Y.G., Yao, B., Li, X.Y., 2025a. Ultrasonic treatment improves the synergistic modification effect of EVA and asphaltenes on nanyang crude oil. Energy Fuel. 39, 10304–10313. https://doi.org/10.1021/acs.energyfuels.5c00568.

Yang, M.P., Li, J.P., Shi, J.K., Zhou, D.X., Yang, C., Li, B.F., Jiao, T.F., 2025b. Preparation and properties of new nano hybrid crude oil pour point depressant. Colloids Surf. A Physicochem. Eng. Asp. 723, 137411. https://doi.org/10.1016/j.colsurfa.2025.137411.

Yang, T.S., Wu, J.J., Yuan, M.X., Li, X., Yin, S.Y., Su, B.T., Yan, J.C., Lin, H.L., Xue, Y., Han, S., 2021. Influence of polar groups on the depressive effects of polymethacrylate polymers as cold flow improvers for diesel fuel. Fuel 290, 120035. https://doi.org/10.1016/j.fuel.2020.120035.

Yang, T.S., Yin, S.Y., Xie, M.Y., Chen, F.F., Su, B.T., Lin, H.L., Xue, Y., Han, S., 2020. Effects of N-containing pour point depressants on the cold flow properties of diesel fuel. Fuel 272, 117666. https://doi.org/10.1016/j.fuel.2020.117666.

Yang, Y.H., Chen, H.L., Sun, Z.N., Bai, M.X., Jing, G.L., Liu, Y., Liu, X.Y., 2025c2025. Preparation and evaluation of poly(octadecyl acrylate-methylbutenol) as a pour point depressant for waxy oil. J. Taiwan Inst. Chem. Eng. 168, 105938. https://doi.org/10.1016/j.jtice.2024.105938.

Yao, B., Li, C.X., Zhang, X.P., Yang, F., Sun, G.Y., Zhao, Y.S., 2018. Performance improvement of the ethylene-vinyl acetate copolymer (EVA) pour point depressant by small dosage of the amino-functionalized poly methyl silses quioxane (PAMSQ) microsphere. Fuel 220, 167–176. https://doi.org/10.1016/j.fuel.2018.01.032.

Yao, Z.M., Zhang, Y.Y., Zheng, Y.Z., Xing, C.H., Hu, Y., 2022. Enhance flows of waxy crude oil in offshore petroleum pipeline: A review. J. Pet. Sci. Eng. 208, 109530. https://doi.org/10.1016/j.petrol.2021.109530.

Yin, S.Y., Yang, T.S., Xue, Y., Xie, M.Y., Chen, F.F., Lin, H.L., Dai, B., Gao, F., Han, S., 2020. Influence of tetradecyl methacrylate-*N*-α-methacrylamide copolymers as pour point depressants on the cold flow property of diesel fuel. Energy Fuel. 34, 11976–11986. https://doi.org/10.1021/acs.energyfuels.0c00890.

Yin, X.N., Liu, H.Z., Yang, C., 2024. Research status and prospect of rheology of waxy crude oil. Chem. Technol. Fuels Oils 60, 954–969. https://doi.org/10.1007/s10553-024-01758-y.

Zhang, J., 2003. Study on performance mechanism of pour point depressants with differential scanning calorimeter and X-ray diffraction methods. Fuel 82, 1419–1426. https://doi.org/10.1016/S0016-2361(03)00028-0.

Zhang, L.N., Sun, Z.N., Jing, G.L., Liu, X.Y., Liu, Y., Yang, Y.H., 2023. Preparation and properties of EVA-g-MAH polymer pour point depressant. Polym. Mater. Sci. Eng. 39, 71–78. https://doi.org/10.16865/j.cnki.1000-7555.2023.0044.

Zhang, X.K., An, X.F., Sun, B., Shui, H.F., Lin, H.L., Han, S., 2022. A novel higher fatty acid-based polymeric cold flow improver with remarkable effects for biodiesel – diesel blends. Ind. Crops Prod. 188, 115471. https://doi.org/10.1016/j.indcrop.2022.115471.

Zhang, X.S., Shi, J.F., Zhao, R.D., Ma, G.Q., Li, Z.Y., Wang, X.F., Zhang, J.K., 2024. Simulation of wellbore pipe flow in oil production engineering: Offshore concentric double-tube CO_2-assisted superheated steam wellbore during SAGD process of heavy oil reservoirs. Energy 294, 130864. https://doi.org/10.1016/j.energy.2024.130864.

Zhu, W.J., Lei, X.W., Wang, H.G., Lin, H.L., Han, S., 2025. Influence of natural aromatic ether extracts (estragole, methyleugenol and α-asarone) on the depressive effects of polymethacrylate copolymers as additives for diesel fuel. Fuel 388, 134546. https://doi.org/10.1016/j.fuel.2025.134546.